Duke Power®

D.M. JAMIL
Vice President

Duke Power
Catawba Nuclear Station
4800 Concord Road / CN01VP
York, SC 29745-9635

803 831 4251

803 831 3221 fax

September 22, 2005

U.S. Nuclear Regulatory Commission
Attention: Document Control Desk
Washington, DC 20555

Subject: Duke Energy Corporation
Catawba Nuclear Station, Unit 2
Docket No. 50-414
Second Ten Year Inservice Inspection Interval
Steam Generator C Hot Leg Nozzle Welds

References: Letters from Duke Energy Corporation to NRC, same subject, dated October 19, 2004 and December 2, 2004

The reference letters transmitted Revisions 0 and 1 of an analytical evaluation of a steam generator hot leg nozzle weld flaw discovered during the Catawba Unit 2 End of Cycle 13 Refueling Outage. The evaluation was contained in WCAP-15658-P, "Flaw Evaluation Handbook for Catawba Unit 2 Steam Generator Primary Nozzle Weld Regions" (Proprietary).

On May 11, 2005, the NRC transmitted a Request for Additional Information (RAI) concerning this analytical evaluation. The purpose of this letter is to respond to this RAI. The RAI response is contained in the attachment to this letter. The format of the response is to restate each RAI question, followed by the response.

There are no regulatory commitments contained in this letter or its attachment.

If there are any questions concerning this information, please contact L.J. Rudy at (803) 831-3084.

A047

Very truly yours,

John Putesa for

D.M. Jamil

LJR/s

Attachment

xc (with attachment):

W.D. Travers
U.S. Nuclear Regulatory Commission
Regional Administrator, Region II
Atlanta Federal Center
61 Forsyth St., SW, Suite 23T85
Atlanta, GA 30303

E.F. Guthrie
Senior Resident Inspector (CNS)
U.S. Nuclear Regulatory Commission
Catawba Nuclear Station

S.E. Peters (addressee only)
NRC Project Manager (CNS)
U.S. Nuclear Regulatory Commission
Mail Stop 0-8 G9
Washington, D.C. 20555-0001

ATTACHMENT

RESPONSE TO NRC REQUEST FOR ADDITIONAL INFORMATION

REQUEST FOR ADDITIONAL INFORMATION

DUKE POWER COMPANY

CATAWBA NUCLEAR STATION, UNIT 2

DOCKET NO. 50-414

The Nuclear Regulatory Commission (NRC) staff has reviewed the licensee's submittals dated October 19 and December 2, 2004, regarding an evaluation of a flaw indication in the reactor coolant hot leg to steam generator nozzle connection, that was discovered on October 7, 2004, during the 13th refueling outage for Catawba Nuclear Station, Unit 2. The NRC staff has identified the following information that is needed to enable the continuation of its review.

1. In the letter dated October 19, 2004, you stated, "[t]he indication was located near the interface between the safe-end and field weld at the bottom of the nozzle." Please confirm whether the flaw indication is in the safe end or in the field weld.

Duke Energy Corporation Response:

The flaw is located at the boundary between the safe end (actually a stainless steel buttering of the carbon steel nozzle) and the stainless steel field weld. A sketch is attached showing the location of the flaw relative to the safe end buttering and the field weld.

CNS Steam Generator 2C Hot Leg Nozzle Indication

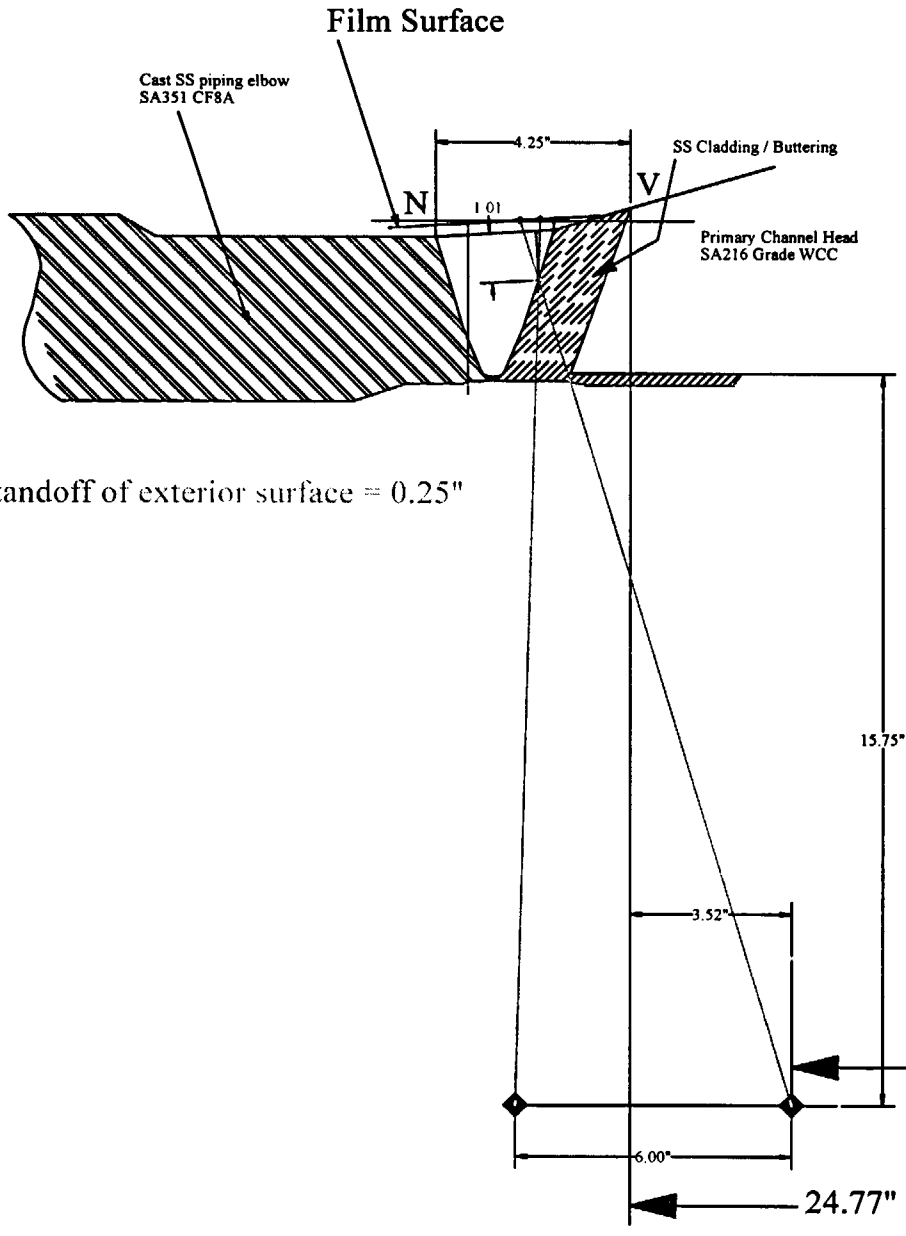

Film standoff of exterior surface = 0.25"

Source Location

21.25" from back of nozzle dam ring

24.77" from back of nozzle dam ring

Reference Drawings:
1) CNM-2201.01-0008
2) CNM-1201.01-0076

2. In the letter dated October 19, 2004, you stated, "[t]his letter submits the fracture mechanics analysis to the NRC (see attachment)". The NRC staff did not find in your submittal an evaluation of the detected flaw indication (1 inch long circumferential embedded flaw, 1.01 inches from the outside diameter of the pipe) using WCAP-15658-P, Revision 1. Please provide this information. The response should include the WCAP figure number (Figure A-4.6, Figure A-4.7, Figure A-4.8, or Figure A-4.9) that you used for evaluation of the detected flaw in the steam generator primary nozzle weld region. The response should also include the depth of the detected flaw (the size of the flaw in the wall thickness direction).

Duke Energy Corporation Response:

Nozzle Configuration

The nozzle connection consists of a low alloy steel casting that forms the channel head of the steam generator. This casting has been buttered with a low carbon, stainless steel weld metal. The piping to buttering field weld is made after post weld heat treatment of the steam generator channel head. The Duke weld number is 2NC-13-2. The weld is a full penetration, compound V groove weld made from the outside of the pipe. The GTAW (TIG) process was used for the first inch, followed by a "courtesy" radiograph (RT). Subsequent welding was performed using the SMAW (stick) process to finish out the weld. After completion of welding, a final RT was performed and accepted on the weld. In addition, liquid penetrant tests (PTs) were performed on the interior and exterior surfaces of the weld.

Flaw Geometry

The flaw is located at the bottom of the pipe in the C hot leg. It is approximately at bottom dead center of the pipe. Based on the radiographic data, the flaw is one inch long and oriented in the circumferential direction. Since the examination was performed using radiographic testing (RT), a limited amount of information was available to characterize the flaw. The location of the flaw relative to the outside diameter surface was established using parallax radiographic shots. These shots support a minimal flaw depth. However, because of the uncertainty in flaw depth, a bounding case has been reviewed herein.

Radiography Evaluation

In addition to the radiography shots made to characterize the flaw, both the original construction film and the End of Cycle 13 film (non-parallax shots) were digitized. The original construction film was digitized to determine if the indication could be seen from initial fabrication welding. Digitization of the film can greatly enhance the visible interpretation of the film in some cases. Next, the End of Cycle 13 film was digitized and reviewed to determine if the linear indication was actually separated into multiple flaws. In both of these cases, there was no conclusive evidence from the digitization process that changed the film interpretation or flaw characteristics.

Based on the conclusions provided from the radiography review above, a best estimate characterization of the flaw has been provided. The flaw is located 1.01 inches from the outside surface of the piping in the stainless steel weld material. The flaw is oriented circumferentially with a length of 1.0 inch. The flaw is most likely the result of a slag inclusion during fabrication. It has very little contrast, which indicates a limited depth. It is located at the interface between the stainless steel buttering and the Duke stainless steel field weld.

The flaw location from the outside diameter surface of 1.01 inches was considered from three positions relative to the flaw depth (top, center, and bottom). The three positions were considered for two different aspect ratios. All six cases were found to be acceptable. Based on the method used to determine location, the center position is the most appropriate and is used in the documented flaw calculation below.

For the initial evaluation, the flaw depth will be assumed as one-half of the length and evaluated as an embedded flaw. From the flaw handbook, several parameters are necessary to determine the acceptability of the indication. These are provided below. The appropriate figure for the purposes of evaluation from WCAP-15658-P, Revision 1 for a circumferential embedded flaw in the stainless steel material is Figure A-3.7.

a	=	half flaw depth (in)
	=	0.25 in
l	=	length of flaw (in)

= 1.0 in

t = wall thickness (in)
= 3.25 in

> Note: The wall thickness is based on profiling of the weld using ultrasonic testing (UT) probe. The value of 3.25 inches is conservative and represents the lowest reading throughout the weld region of interest.

δ = distance to flaw centerline
= 1.01 in

δ / t = 1.01 / 3.25
= 0.311

a / t = 0.25 / 3.25
= 0.077

The δ / t and a / t parameters may be plotted on Figure A-3.7 to determine the acceptability of the flaw. This point (A) is shown on the attached sketch.

In addition to the above evaluation, the flaw depth was increased to 1 inch yielding an aspect ratio of 1:1. In this case, the parameters change as noted below:

a = half flaw depth (in)
= 0.50 in

l = length of flaw (in)
= 1.0 in

t = wall thickness (in)
= 3.25 in

δ = distance to flaw centerline
= 1.01 in

δ / t = 1.01 / 3.25
= 0.311

a / t = 0.50 / 3.25
= 0.154

Again, the δ / t and a / t parameters have been plotted on Figure A-3.7 as point (B) to determine the acceptability of the flaw.

CATAWBA 2 STEAM GENERATOR INLET NOZZLE STAINLESS STEEL PIPE WELD CIRCUMFERENTIAL EMBEDDED FLAW EVALUATION CHART

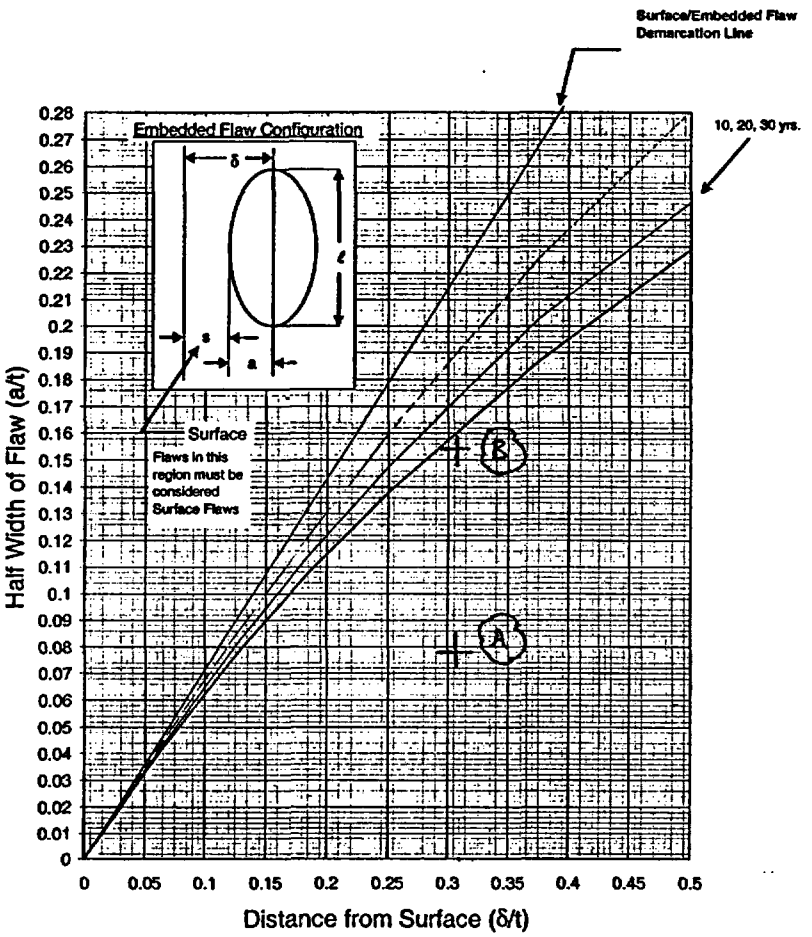

X Inside Surface	___Surface Flaw	___Longitudinal Flaw
X Outside Surface	X Embedded Flaw	X Circumferential Flaw

Figure A-3.7 Evaluation Chart for Steam Generator Inlet Nozzle Safe-End to Pipe Weld (Stainless Steel)

CNC-2201.01-00-0006, Rev 0
Page 7

Orig: WOC 10-12-04
Chk: GJW 10-13-04

Results

In both cases evaluated above, it is clearly evident that the flaw is within the bounds of the acceptability provided by Figure A-3.7 of WCAP-15658-P, Revision 1. As a result, the piping containing this flaw is acceptable for continued service for the design life of the plant. The figure in WCAP-15658-P, Revision 1 indicates 10, 20, and 30 year acceptance lines. These lines are related to the design number of occurrences of transients used in the fatigue crack growth calculation. As such, this indication is acceptable for the life of the plant provided a prorated value (30 / 40 = 75%) of the design number of occurrences are not exceeded between now and the end of plant life. This limit on fatigue cycle counts will be tracked under our fatigue management program.

Conclusion

The flaw discovered during End of Cycle 13 is acceptable without repair for the life of the plant. Acceptance by the performance of analytical evaluation as allowed by ASME Section XI, IWB-3132.4 has been validated. Additional examinations have been performed during End of Cycle 13 to satisfy IWB-2430. Successive examinations for the SG 2C hot leg weld number 2NC-13-2 will be necessary in the subsequent three ISI periods as required by IWB-2420.

3. On Page 3-1 of WCAP-15658-P, Revision 1, "Flaw Evaluation Handbook for Catawba Unit 2 Steam Generator Primary Nozzle Weld Regions," November 2004", it is stated, "[t]he stress intensity factor calculation for an embedded flaw was taken from the work by Shah and Kobayashi [6] which is applicable to an embedded flaw in an infinite medium …. This expression has been shown to be applicable to embedded flaws in a thick-walled pressure vessel in a paper by Lee and Bamford [7]." Please demonstrate the applicability of Kobayashi's formulas for embedded flaws to your current application by addressing (1) the difference between the finite geometry of the current application and an infinite medium discussed in Kobayashi's paper, and (2) the difference between the ratio of plate thickness to crack depth, t/2a, of the current application and that discussed in Kobayashi's paper. Provide Reference 7 of WCAP-15658-P, Revision 1 (Paper 83-PVP-92 by Lee and Bamford) if you believe it would help your explanation.

Duke Energy Corporation Response:

Note: The response to this question was developed by Westinghouse. Refer to the enclosed Westinghouse material for the additional information to support this response.

The Lee and Bamford paper is attached for your information (Enclosure 1), and should provide a sufficient basis for the use of the Shah and Kobayashi closed form solution for the embedded flaw. This work was done for the express purpose of deciding whether a closed form solution was sufficient to model embedded flaws in finite thickness geometries, and the conclusion was that the closed form solution was indeed good for this application. This conclusion was reached by setting up a series of finite element geometries and loadings, and comparing the weight function results with the closed form solutions of Shah and Kobayashi. The detailed comparisons are provided in the paper.

4. On Page 3-4 of WCAP-15658-P, Revision 1, it is stated, "NRC procedures exist for addressing the impact of thermal aging on fracture toughness for full-service life. The approved procedures were applied to the nozzle safe end to pipe weld, as well as to the cast piping itself." Provide the specific document (e.g., NUREG number) and parameters used (e.g., ferrite content) in your determination of fracture toughness for full-service life using NRC procedures. Explain how you use these NRC procedures to determine the first set of proprietary J_{1c} and T_{mat} given on Page 3-4. It is further stated on this page, "[e]ven with thermal aging, equivalent to full service for SAW welds, the tearing modulus remains high (>100) and the unaged toughness, J_{1c}, is not significantly reduced." Provide information supporting this statement.

Duke Energy Corporation Response:

Note: The response to this question was developed by Westinghouse. Refer to the enclosed Westinghouse material for the additional information to support this response.

The cover letter transmitting the first SER issued by NRC on this subject is attached (Enclosure 2); many others have been issued over the years which provide a similar

endorsement of the Westinghouse approach. This approach was developed over an extended period of time with Westinghouse internal funding, and included interactions with the Staff on many occasions to clarify the methodology, so it was important to keep the methodology out of the public literature. Westinghouse has used this same approach to describe the assessment of thermal aging which was done for a number of different flaw evaluations, over a period of many years.

ENCLOSURE 1

LEE AND BAMFORD PAPER

THE AMERICAN SOCIETY OF MECHANICAL ENGINEERS
345 E. 47 St., New York, N.Y. 10017

83-PVP-92

STRESS INTENSITY FACTOR SOLUTIONS FOR A LONGITUDINAL BURIED ELLIPTICAL FLAW IN A CYLINDER UNDER ARBITRARY LOADS

Y. S. Lee, Mem. ASME
W. H. Bamford, Mem. ASME

Westinghouse Electric Corporation
Nuclear Energy Systems
P.O. Box 355
Pittsburgh, Pennsylvania 15230

ABSTRACT

Elastic stress intensity factor solutions were obtained for a buried elliptical flaw of major to semi-minor axis ratio 6, located in the longitudinal plane of a cylinder of radius to thickness ratio 10. The flaws were located at distances of 3/16, 1/4, 1/2 and 3/4 times the wall thickness from the inside of the cylinder wall. The results were compared with those for an infinite elastic medium available in the literature. The results presented in this report show that the infinite medium solutions can be used for evaluation of cylindrical vessel geometry considered in this report for flaws located within 25 to 75 percent of the wall thickness. For flaws located outside this region the stress intensity factors appear to increase. A comparison between the ASME Section XI membrane correction factors and those of this work shows that the former are conservative for the eccentricity limit specified in the code.

INTRODUCTION

The buried elliptical flaw is one of the most common flaw types found in many structure. Accurate stress intensity factor expressions under all applicable loading conditions are necessary to establish the actual safety margin. Longitudinal buried flaw in a thick-walled cylinder is of particular interest because of its application in the structural integrity evaluation of reactor vessel beltlines.

Many investigators have studied the surface flaw in cylinder. Due to the perceived difficulties of three dimensional analysis, the early investigators assumed the flaw to be continuous and used two dimensional analysis. Bowie and Freese[1] studied a continuous longitundinal flaw in a cylinder under pressure. This work was generalized to both continuous longitudinal and continuous circumferential flaws in a thick cylinder under arbitrary loadings by Buchalet and Bamford[2] and Labbens, et al.[3] Initial attempts to approximate solutions for the full three dimensional problem were made by Underwood[4] and Kobayashi.[5] Neither Underwood or Kobayashi included the effect of the outside surface of the cylinder. For example, Underwood[4] assumed that the effect of a given crack shape on K_I (stress intensity factor) of a pressurized cylinder is the same as that due to the shape effect on the K_I of a plate under uniform tension. Kobayashi et al[6,7,8] have estimated K_I for a longitudinal semi-elliptical surface flaw in a cylinder under both pressure and thermal shock loadings. In this study, the authors determined the solutions for flaws in cylinder from the solution for similar flaws in flat plates subjected to identical stress profiles. The flat plate results were then modified with curvature correction factors obtained from a two-dimensional analysis. Both front and back surface effects were considered, but the curvature correction factors were most accurate for only the deepest point along the semi-elliptical flaw.

More recently direct three-dimensional solutions to the semi-elliptical surface flaw problem in a cylinder have been obtained by several investigators. Among these are the results reported by Ayers,[9] Blackburn and Hellen,[10] and Atluri, et al.[11,12] Ayers used a condensed quarter-point element to determine the stress intensity factor distribution of two semi-elliptical flaws in a thermally shocked cylinder with ratio of outer to inner radius equal to 1.90. Blackburn and Hellen used a conventional three-dimensional finite element code and a virtual crack extension procedure to determine the stress intensity factor expressions for inner and outer surface flaws in cylinders under pressure with the ratio of outer to inner radius equal to 1.461. Alturi used a hybrid-displacement crack tip element to determine the stress intensity factor distribution around the flaw border of semi-elliptical flaw in pressurized cylinders with the ratio of outer to inner radius equal to 1.5 and 2.0. For the same geometries, these direct three-dimensional approaches all give similar results (approximately 10 percent variance).

As noted above, the geometries treated in the full three-dimensional manner are only for limited loading

conditions and for geometries that are widely different from commercial pressure vessels (ratio for outer radius to inner radius is 1.1). To verify the structural integrity of these pressure vessels, a considerable range of loading conditions were investigated by McGowan and Raymund.[13] They assumed the aspect ratio of the flaw to be 6.0 as recommended by the ASME Boiler and Pressure Vessel Code, Section III, Appendix G.[14] Using boundary integral equation method, Heliot, Labbens, and Pellissier-Tanon[15] solved the identical problem and obtained results which agreed well with the macroelement results. More recently, Newman and Raju[16] obtained stress intensity factor solutions for a wide range of semi-elliptical surface cracks on the inside of pressurized cylinders.

Investigations of the fracture mechanics characteristics of the buried elliptical flaw have not been undertaken as extensively as those for the surface flaw. Kobayashi, et al[17] and Ishida[18] obtained correction factors for a buried flaw in an infinitely long strip subjected to membrane stress loading. A comparison of the results obtained by Kobayashi, et al[17] and Ishida[18] shows that the results differ by a wide margin depending on the location of the crack and the ratio of the flaw minor axis to the strip thickness. The largest difference were observed for both larger values of eccentricity (measured in terms of distance between the flaw axis and the strip center line) and ratio of crack depth (minor axis) to strip thickness. Shah and Kobayashi[19] obtained in analytical expression for the stress intensity factor for a buried elliptical flaw in an infinite medium subjected to an arbitrary internal pressure using three-dimensional elasticity theory.

Naturally, Shah-Kobayahsi[19] solution did not contain curvature effects. The objective of the present analysis is to obtain the stress intensity factors (or magnification factors) for buried elliptical flaws at various locations in the longitudinal cross-section of a finite thickness vessel. The aspect ratio defined by the ratio of the flaw major axis to semi-minor axis employed in this analysis is 6.0 as recommended by the ASME Boiler and Pressure Vessel Code, Section III, Appendix G.[14] The ratio of outer to inner radius of the cylinder is 1.1. The stress intensity factor solution is obtained by the Macroelement Technique developd by Hall, Raymund and Palusamy.[20] This method have been shown to give good results for various three-dimensional crack problems as reported by Palusamy and Heliot.[21] The stress intensity factor distribution around the elliptical crack front is calculated using the "stiffness derivative" procedure as proposed by Parks.[22]

The physical dimensions of the buried flaws considered in this study is identical to an ellipse with major and minor axes of 3/4 and 1/4 vessel wall thickness, respectively. Stress intensity factor solutions are presented for the flaws located at three-sixteenth, one-quarter, one-half and three-quarter positions of the vessel wall and subjected to constant, linear, quadratic and cubic distributions of crack surface loadings. These results are then compared to the corresponding results obtained by Shah and Kobayashi[19] for infinite medium. Comparisons are also presented between the present results and those due to the Appendix A of the Section XI of the ASME Boiler Code.[23]

Problem Statement

Shown in Figure 2-1 is a cylindrical pressure vessel containing a buried flaw in the longitudinal cross-section of the vessel wall. The buried flaw shape is assumed to be elliptical, as shown in Figure 2-1, with major and minor axis of 2c and 2a, respectively. In this investigation, the aspect ratio of the flaw, defined by the ratio of the major axis to the semi-minor axis (2c/a), is assumed to be 6. The flaw is assumed to be located in the longitudinal cross-section of the wall of a cylinder with dimensions representing Pressurized Water Reactor (PWR) vessel beltline. The inside and thickness are R_i and T, respectively. The ratio of R_i/T is chosen to be 10. The dimensional values chosen for R_i and T are 65 in. and 6.5 in., respectively. The stress intensity factor solutions are obtained for the buried flaw located in four positions in the longitudinal cross-section shown in Figure 2-1. The flaw location is defined by the distance, ξT, measured between the inside surface of the cylinder and the flaw major axis. The values of ξ chosen for this investigation are 3/16/, 1/4, 1/2 and 3/4. The ligament thickness measured, respectively, from the inside and outside surfaces of the vessel are represented by ξ_i and ξ^o.

The stress intensity factor solutions for the buried flaw are sought for four different crack opening pressure loadings, $\sigma(x)$ defined by:

$$\sigma(x) = A_0 \quad (2.1)$$
$$\sigma(x) = A_1 x \quad (2.2)$$
$$\sigma(x) = A_2 x^2 \quad (2.3)$$
$$\sigma(x) = A_3 x^3 \quad (2.4)$$

where A_0, A_1, A_2 are arbitrarily coefficients and x is the coordinate defined in Figure 2-1.

MACROELEMENT TECHNIQUE

A detailed formulation of the macroelement technique developed by Hall, Raymund and Palusamy is contained in [20]. The macroelement technique consists of dividing the flawed three-dimensional structure into two or more substructures and modeling the region containing the flaw by one or more macroelement substructures. The solution process begins by obtaining a condensed stiffness matrix for each of the substructures followed by global displacement solution. The mode I crack-tip stress intensity factors (K_I) are then determined from the displacement solution using Parks' stiffness derivative [22] method.

The macroelement is built out of 45 microelements of which 37 are blended bricks and 8 are wedge elements, Figure 3.1. The details of these microelements are contained in [20], and it suffices to know that the wedges have 45 degrees of freedom (d.o.f.), and the d.o.f. of blended bricks can be varied subject to minor restrictions specified in [20]. The undeformed macroelement shown in Figure 3.2 contains a built-in quarter-elliptical crack. The region surrounding the crack tip is modeled by a channel of 28 blended bricks enabling the analyst to vary the density of nodes to achieve a desired combination of accuracy and cost. The total of d.o.f. corresponding to the choice of minimum density is 1296.

The principal characteristics of the macroelement are the following: it is compatible with the 20-node isoparametric element; it has the option to vary

crack tip region nodal density: it is parametrically defined so as to allow curved faces: it permits a wide variety of crack surface loadings (any combination of terms of a bivariable cubic polynominal), and it significantly reduces the man-time needed to formulate the finite element model.

FINITE ELEMENT MODEL

The finite element model of the reactor vessel beltline containing the buried flaw consisted of a 45° sector of the beltline of length 69 inches and of thickness 6.5 inches. Taking advantage of the symmetry condition, only one half of the flaw was modeled. The crack tip region was modeled by two macroelements and each one was treated as one substructure. The remaining region called mother structure was modeled using 20-node isoparametric brick and 15-node isoparametric wedge elements. A typical finite element model (for ξ = 1/2) is shown in Figure 4-1.

The details of finite element models 1 through 4 corresponding to ξ equal to 3/16/, 1/4, 1/2 and 3/4, respectively, are presented in Table 4.1 A typical model used for the buried flaw located at ξ = 1/2 is shown in Figure 4.1. This model consists of 7 layers of elements each in the circumferential and axial directions. The first layer defined by $\theta = \theta_c$ contains the macroelements. The dimensions of the macroelement in the axial and radial directions are denoted by L_c and W_c. The values of W_c, L_c and θ_c were chosen to be 3 inches, 1.791° and 2.031 inches, respectively, for all four locations. For the case of ξ equal to 0.5, the value of W_c was chosen to be 0.609.

As reported previously each of the macroelement is treated as a separate substructure and contained 45 microelements. The combined macroelement degrees of freedom varied from 3045 to 3384. The number of elements in the mother structure (the third structure) ranged from 173 to 194. One of the features of the Macroelement Technique is that the number of crack tips nodes can be chosen at will subjected to minor restrictions specified in Reference 20. In this investigation each of the macroelements had 25 crack tip nodes.

The first verification of this method was made with reference to a plate containing a semielliptical surface flaw of aspect ratio, 5, fractional through-wall depth, 0.6, and subjected to remote uniform tension loading. It has been shown that the K_I values obtained by the macroelemept technique agreed with those of Raju and Newman[24] and Smith and Sorensen[25] within 3 and 8 percent, respectively. Recently, the macroelement technique has been successfully applied to the Battelle bench mark problem [26] on surface cracked plate [27], semielliptical surface cracks in a cylinder [13] and a single quarter-circular corner cracked hole in a plate [28].

DETERMINATION OF STRESS INTENSITY FACTOR SOLUTION

The stress intensity factor determination using macroelement is carried out in essentially four steps. First, the condensed stiffness matrices were obtained for each of the three substructures. Secondly, these three substructures were connected, the prescribed loads were applied and a global displacement solution was obtained. Thirdly, given the global displacement solution, local displacement solution was obtained for each of the microelements. Finally Parks' [22] stiffness derivative technique was applied to determine the stress intensity factor at each of the crack tip nodes. This process was carried out for each of the load components individually and the stress intensity factor were determined which were then combined based on superposition principle to obtain the stress intensity factor solution for a combined loading.

Experience shows that a third degree polynominal obtained by the summation of loadings defined by Equation (2.1-4) is adequate to represent the stress distribition in the cross-section of a PWR beltline under all operatin conditions of loadings including postulated accident condition loading. Therefore the crack opening hoop stress σ can he represented as follows:

$$\sigma = A_0 + A_1 x + A_2 x^2 + A_3 x^3 \qquad (5.1)$$

The resulting stress intensity factor K_I is then expressed using the principle of superposition as follows:

$$K_I(\phi) = K_{I0}(\phi) + K_{I1}(\phi) + K_{I2}(\phi) + K_{I3}(\phi) \qquad (5.2)$$

where K_{I0}, K_{I1}, K_{I2} and K_{I3} are the stress intensity factor valued due to each of the loadings. It is convenient to express K_I as a function of elliptical angle θ in the following familiar form:

$$K_I(\phi) = M(\phi,a,c)[A_0 H_0(\phi) + \frac{2a}{\pi} A_1 H_1(\phi) \qquad (5.3)$$

$$+ \frac{a^2}{2} A_2 H_2(\phi) + \frac{4\pi a^3}{3} A_3 H_3(\phi)]$$

where the function ν (ϕ, a, c) represents the stress intensity factor factor for a buried elliptical flaw of major axis, 2c and minor axis, 2a in an infinite medium subjected to a uniform crack opening stress of unit magnitude and is defined by [29]

$$M(\phi,a,c) = \frac{\pi a}{Q} (\cos^2\phi + \frac{a^2}{c^2} \sin\phi)^{1/4} \qquad (5.4a)$$

$$Q = \int_0^{\pi/2} (\cos^2\phi + \frac{a^2}{c^2} \sin^2\phi)^{1/2} d\phi \qquad (5.4b)$$

The quantities $H_0(\phi)$, $H_1(\phi)$, $H_2(\phi)$ and $H_3(\phi)$ are magnification factors of position along the crack front and are obtained by comparing Equations (5-2) and (5-3) as follows:

$$H_0(\phi) = \frac{K_{I0}(\phi)}{A_0 M(\phi,a,c)} \qquad (5.5a)$$

$$H_1(\phi) = \frac{K_{I1}(\phi)}{\frac{2a}{\pi} A_1 M(\theta,a,c)} \qquad (5.5b)$$

$$H_2(\phi) = \frac{K_{I2}(\phi)}{\frac{\sigma_2}{\pi} A_2 M(\phi,a,c)} \qquad (5.5c)$$

$$H_3(\phi) = \frac{K_{I3}(\phi)}{\frac{4\sigma_3 a}{3} A_3 M(\phi,a,c)} \qquad (5.5d)$$

A diagramatic description of the load components and the associated magnification factors are shown in Figure 5-1.

STRESS INTENSITY FACTOR RESULTS

Magnification factors were obtained for 6 to 1 aspect ratio (3 to 1 major to minor axis ratio) buried elliptical flaws located at ζ = 3/16, 1/4, 1/2 and 3/4. The results obtained for the magnification factors H_0, H_1, H_2 and H_3 are presented in Figures 6-1 through 6-4. The values of magnification factors vary as a function of elliptical angle, θ. The positions defined by θ equal to 0° and 180° are the farthest and nearest locations on the crack minor axis with respect to the inside surface of the vessel wall. For all positions the factor H_0 is the least varying with respect to θ and the value is about unity. The fact that the value of H_0 is about unit suggests that the influence due to curvature and boundary surface may not be very significant for these cases.

A comparison of the values of respective magnification factors due to various positions shows that the respective values for positions defined by ζ = 1/4, 1/2 and 3/4 are the same within 2 percent. For the positions ζ equal to 3/16, the values of H_0 are about 7, 0 and 12 percent higher at φ equal to 0°, 90° and 180° than the respective values due to other positions. The value of H_2 due to ζ equal to 3/16 are found to be about 7, 0 and 9 percent at φ equal to 0°, 9° and 180° than the respective values due to other positions. A similar but a smaller increase in the values of H_1 and H_3 due to ζ equal to 3/16 are found and these percentage increases are summarized in Table 6-1.

Since there was virtually no difference in the results obtained for positions ζ equal to 1/4, 1/2 and 3/4, question was raised whether there will be any difference between this set of results and those for a similar flaw in an infinite medium. Shah and Kobayashi [19] have reported a general stress intensity factor solution for a buried elliptical flaw in an infinite medium and subjected to a two-dimensional third order crack surface loadings.

From this closed form solution, the values for the the magnification factors H_0, H_1 H_2 and H_3 were derived for a 6 to 1 aspect ratio flaw buried in an infinite medium and are presented in Figure 6.5. Comparisons are shown in Table 6-2 for ζ equal to 0°, 90° and 180°. The last column of this table shows the ratio of the macroelement calculated values for the cylinder geometry over the closed form results obtained for an infinite elastic solid by Shah and Kobayashi [19]. Specifically, for this comparison macroelement results due to ζ equal to 1/2 was used. The values at φ equal to 0° and 180° are lower than those due to the infinite medium values. The deviations range from 8 to 16 percent lower. Another observation is that the macroelement results are symmetric with respect to the major axis of the (flaw) ellipse within about 2 percent. Since no mesh convergence studies were made as it is required in any finite element analysis for establishing the accuracy of the numerical results, the question remains whether the lower values obtained for the cylinder geometry is either due to real effects arising from either curvature and free boundary conditions or inadequate finite element modeling. In general, mesh convergence studies using macroelement are expensive and therefore it is not performed. However, a number of solutions by this technique have been compared with results obtained by other investigators [20,13,21,28]. These comparisons show that the macroelement results can be lower by about 5 to 10 percent.

In order to quantify the discrepancy the macroelement technique was applied to the buried flaw in an infinite medium. All the four loading cases were analyzed. The resulting magnification factors are compared with the solution due to Shah and Kobayashi [19] in Figures 6-6 through 6-9. The values of H_0, H_1, H_2 and H_3 at φ equal to 0, 90 and 180 degrees due to the macroelement method are compared with those due to Shah-Kobayashi method in Table 6-3. The deviations range from -16 percent for H_3 to 13 percent for H_1. It should be noted that these deviations occur at φ equal to 0 or 180 degrees whereas the deviations corresponding to 90 degrees is 2 percent for H_0 and zero percent for H_1, H_2 and H_3. In general, whereas the deviation at 90 degree location is consistent with previous macroelement results (13, 20, 28), the deviations at 0 and 180 degrees are somewhat larger than expected. It is believed that the larger than expected deviation is due to inaccurate mapping of microelements in these locations.

In Figure 6.10, the membrane correction factors obtained for a cylinder of radius to thickness ratio 10 are compared with the ASME Section XI [23] values derived from a plate solution. The comparison shows that the ASME Section XI values are conservative for the range specified in the code (2c/T = 0.6, Figure 6.10) and the extrapolation of this value beyond the specified limit may not be conservative.

SUMMARY AND CONCLUSIONS

Elastic stress intensity factor solutions were obtained for a buried elliptical flaw of aspect ratio 6 (major to minor axis ratio 3), located in the longitudinal plane of a cylinder of radius to thickness ratio 10. The flaws were located at distances of 3/16, 1/4, 1/2 and 3/4 times the wall thickness from the inside of cylinder wall. The macroelement technique of the three-dimensional finite element analysis was used in obtaining the numerical results. The loading on the crack surface consisted of a crack opening pressure field represented by a one-dimensional third order polynomial. The accuracy of the macroelement results as well as the effect of curvature and free boundary were investigated by comparing the results of the macroelement three-dimensional finite element analysis with the closed form results obtained for an

identical flaw located in an infinite elastic medium and subjected to identical loading conditions. The results of this evaluation investigation lead to the following conclusions:

1. A comparison of magnification factors for the cylinder and infinite elastic medium shows that, for flaws located within 25 to 75 percent of the wall thickness, the stress intensity factors agree within + 3 percent. Therefore in this region the infinite elastic medium solution can be used for engineering fracture mechanics evaluation of cylindrical vessels of comparable geometry.

2. For flaws located outside of the region defined by 25 to 75 percent wall thickness, the stress intensity factor appears to increase at 0 and 180 degree locations as the flaw gets closer to the surface. For the one case analyzed where the flaw was considered to be located at a distance of 18.7 percent of wall thickness from the inside, the magnification factors were higher by percentages ranging from 2 to 12 percent. No increase was observed at the 90 degree location.

3. A comparison between macroelement and closed from results from a buried elliptical flaw in an infinite elastic solid medium confirms the previously published conclusions that the macroelement method can give results that are accurate within 5 to 10 percent at 90 degree locaton. However, the inaccuracies at 0 and 180 degree location have been observed to be as large as 15 percent.

4. A comparison between the ASME Section XI membrane correction factors and the macroelement correction factors shows that the former values are conservative for the eccentricity limit specified in the code and that the extrapolation of the current code values may not be conservative.

REFERENCES

1. Bowie, O. L. and Freese, C. E., "Elastic Analysis for a Radial Crack in a Circular Ring", Engineering Fracture Mechanics, Vol. 4, No. 2, pp. 315-322, June 1972.

2. Buchalet, C. B. and Bamford, W. H., "Stress Intensity Facotr Solutions for Continuous Surface Flaws in Reactor Pressure Vessels", Mechanics of Crack Growth, ASTM-STP-490, pp. 385-402, American Society for Testing and Materials, Philadelphia, 1976.

3. Labbens, R., Pellissier-Tanon, A., and Heliot, J., "Practical Method for Calculating Stress-Intensity Factors Through Weight Functions", Mechanics of Crack Growth, ASTM-STP-590, pp. 368-384, American Society for Testing and Materials, Philadelphia, 1976.

4. Underwodd, J. H., "Stress Intensity Factors for Internally Pressurized Thick-Walled Cylinders", Stress Analysis and Growth of Cracks, ASTM-STP-513, pp. 59-70, American Society for Testing and Materials, Philadelphia, 1972.

5. Kobayahsi, A. S., "A Simple Procedure for Estimating Stress Itensity Factors in Regions of High Stress Gradients", Significance of Defects in Welded Structures (ed. T. Kanazawa and A. S. Kobayashi), pp. 127-43, University of Tokyo Press, 1974.

6. Kobayashi, A. S., Polvanich, N., Emery, A. F., and Love, W. J., "Stress Intensity Factor of a Surface Crack in a Pressurized Cylinder", Computation al Fracture Mechanics, June, 1975.

7. Kobayashi, A. S., Emery, A. F. Polvanich, N., and Love, W. J., "Surface Flaw in an Pressurized and Thermally Shocked Hollow Cylinder", Int. J. Press Ves. and Piping, Vol. 5, pp. 103-122, 1977.

8. Kobayahsi, A. S., A. F., Polvanich, N., and Love, W. J., "Inner and Outer Surface Cracks in Internally Pressurized Cylinders", J. Press. Ves. Tech., ASME pp. 83-89, Feb. 1977.

9. Ayers, D. J., "Three-Dimensional Elastic Analysis of Semi-Elliptical Surface Flaws Subjected to Thermal Shock", Computational Fracture Mechanics, ASME, (ed. E. F. Rybicki and S. E. Benzley), pp. 133-143, 1975.

10. Blackburn, W. S. and Hellen, T. K., "Calculation of Stress Intensity Factors for Elliptical and Semi-Elliptical Cracks in Blocks and Cylinders", Central Electricity Generating Board Report No. RD/B/N3103, July 1974.

11. Atluri, S. N., Kathiresan, K., Kobayashi, A. S., and Nakagaki, M., "Inner Surface Cracks in an Internally Pressurized Cylinder Analyzed by a Three-Dimensional Displacement-Hybrid Finite Element Method", Proceedings of the Third International Conference on Pressure Vessel Technology (Tokyo, Japan, April 19-22, 1977), ASME, pp. 527-53.

12. Atluri, S. A., and Kathiresan, K., "Outer and Inner Surface Flaws in Thick-Walled Pressure Vessels", paper G 5/4 Transactions of the Fourth International Conference on Structural Mechanics in Reactor Technology, San Francisco, Cal. 1977.

13. McGowan, J. J. and Raymund, M., "Stress Intensity Factor Solutions for Internal Longitudinal Semi-elliptical Surface Flaws in a Cylinder Under Arbitrary Loading", STP-677, ASTM, Philadelphia, 1979, pp. 365-380.

14. ASME Boiler and Pressure Vessel Code, Section III, App. G "Protection Against Nonductile Failure", 1980.

15. Heliot, J., Labbens, R. C. and Pellissier-Tanon, A., "Semi-elliptical Cracks in a Cylinder Subjected to Stress Gradients", STP-677, ASTM, 1978, pp. 341-364.

16. Newman, Jr., J. C., and Raju, I. S., "Stress-Intensity Factors for Internal Surface Cracks in Cylindrical Pressure Vessels", Trans. ASME, J. of Pressure Vessel Tech., 102, 1980, pp. 342-346.

17. Kobayashi, A. S., Ziv, M. and Hall, L. R., "Approximate Stress Intensity Factor for an Embedded Elliptical Crack Near Two Parallel Free Surfaces" International Journal of Fracture Mechanics Vol. 1, 1965, p. 81-95.

18. Ishida, M., "Stress Intensity Factors for the Tension of an Eccentrically Cracked Strip", Journal of Applied Mechanics, Sept. 1966, p. 674-675.

19. Shah, R. C. and Kobayashi, A. S., "Stress Intensity Factor for an Elliptical Crack Under Arbitrary Loading", Engineering Fracture Mechanics, Vol. 3, 1971, p. 71-96.

20. Hall, C. A., Raymund, M. and Palusamy, S. S., A Macroelement Approach to Computing Stress Intensity Factor for Three-Dimensional Structures", Int. J. Frac., Vol. 15, No. 3, 1979, pp. 231-245.

21. Palusamy, S. S. and Heliot, J., Two Stress-Intensity Factor Calculation Methods and Solutions for Various Three-Dimensional Crack Problems, presented in the 5th Intl. Conf. on Frac., CANNES, France, 1981.

22. Park, D. M., "A Stiffness Derivative Finite Element Technique for Determination of Crack Tip Stress Intensity Factors", International Journal of Fracture, Vol. 10, 1974, pp. 487-502.

23. ASME, Boiler and Pressure Vessel Code, Section XI, Appendix A, 1977 Edition.

24. Raju, I. S. and Newman, J. C., Jr., "Stress Intensity Factors for a Wide Range of Semi-Elliptical Surface Cracks in Finite Thickness Plates, Engineering Fracture Mechanics, Vol. II, 1979, pp. 817-829.

25. Smith, F. W., and Sorensen, D. R., "The Semi-Elliptical Surface Crack - A Solution by the Alternating Method," International J. of Fracture, Vol. 12, 1976, pp. 47-57. Also see Colorado State Univ. Tech. Report 4, NASA Grant NGL-06-002-063, 1973.

26. Hulbert, L. E., "Benchmark Problems for 3-D Fracture Analysis", Int. Jl. of Fracture, 13, 1977, pp. 87-91.

27. McGowan, J. J. and Raymund, J. J., "Stress Intensity Factor Solutions for Surface Flaws in Finite Thickness Plates under Arbitrary Loading WCAP 9318, Westinghouse Electric Corporation, Pittsburgh, PA April 1978.

28. Palusamy, S. S. and Raymund, M., "Stress Intensity Factor of Corner Crack at the Edge of a Hole in a Plate", STP 743, ASTM, Philadelphia, PA 1981.

29. Sadowsky, M. A., "Stress Concentration Around a Triaxial Ellipsoidal Cavity", Trans. ASME J. of App. Mech., 1949.

APPENDIX I

STRESS INTENSITY FACTOR SOLUTION FOR ONE DIMENSIONAL STRESS DISTRIBUTION OBTAINED FROM SHAH-KOBAYASHI RESULTS

This section discusses the derivation of the reduced stress intensity factor expression obtained from the general solution presented by Shah-Kobayashi [19]. The reduced stress intensity factor expression was required to compare the results obtained by Shah and Kobayashi [19] with those obtained in this report.

The normal stress σ_z at z = 0 which is perpendicular to the crack plane x and y is expressed as:

$$\sigma_z\Big|_{z=0} = \frac{\partial^2\phi}{\partial z^2}\Big|_{\lambda=0} = \frac{p(x,y)}{2G} = \frac{1}{2G}\sum_{\substack{m=0\\n=0}}^{3} A_{nm}(C_{ij})y^m x^n \quad \text{(A-1)}$$

$$\text{if } x = 0 \text{ then } \sigma_z\Big|_{\lambda=0} = \frac{1}{2G}\sum_{m=0}^{3} A_{om}\, y^m$$

where ϕ is stress function and

λ = one of the ellipsoidal coordinate system
$p(x,y)$ = arbitrary loading in x-y plane
G = shear modulus of a medium
x = major axis
y = minor axis

The stress function ϕ is expressed in terms of the higher derivatives of the potential function with respect to x and y which is known.[19] Therefore $\partial^2\phi/\partial z^2\,|_{\lambda=0}$ is obtained through the algebraic operations.

In equation (A-1) the unknown constants C_{ij} in $\partial^2\phi/\partial z^2\,|_{\lambda=0}$ are obtained by equating the coefficients of y^m which are A_{om} and thos eof y^m in $\partial^2\phi/\partial z^2\,|_{\lambda=0}$. A more detailed derivation and explanation is given in reference [19].

The coefficient, A_{00} in equation (A-1) is equal to that in $\partial^2\phi/\partial z^2\,|_{\lambda=0}$ and it is given as:

$$\frac{1}{2G}A_{00} = \alpha_{11}C_{00} + \alpha_{14}C_{20} + \alpha_{16}C_{02} \quad \text{(A-2)}$$

The coefficient, A_{10} is equation (A-1) is:

$$\frac{1}{2G}A_{10} = \alpha_{22}C_{10} + \alpha_{27}C_{30} + \alpha_{29}C_{12} = 0 \quad \text{(A-3)}$$

Repeating the above procedure, the following simultaneous equations are established:

$$\begin{aligned}
&1/2G\ A_{01} = \alpha_{33}C_{01} + \alpha_{38}C_{21} + \alpha_{310}C_{03}\\
&1/2G\ A_{20} = 0 = \alpha_{44}C_{20} + \alpha_{46}C_{02} \quad \text{(A-4)}\\
&1/2G\ A_{11} = 0 = \alpha_{55}C_{11}\\
&1/2G\ A_{02} = \alpha_{64}C_{20} + \alpha_{66}C_{02}\\
&A_{21}/2G = 0 = \alpha_{88}C_{21} + \alpha_{810}C_{03}\\
&A_{12}/2G = 0 = \alpha_{97}C_{30} + \alpha_{99}C_{12}\\
&A_{03}/2G = \alpha_{108}C_{21} + \alpha_{1010}C_{03}\\
&A_{30}/2G = 0 = \alpha_{77}C_{30} + \alpha_{79}C_{12}
\end{aligned}$$

where α_{ij} are known and are defined by equations (A-7) and (A-8) to follow.

From equations (A-2), (A-3), and (A-4), C_{ij} can be expressed in terms of A_{ij} and α_{ij} by solving the simultaneous equations. The solutions of C_{ij} are:

$$C_{11} = C_{30} = C_{12} = C_{10} = 0$$

$$C_{00} = \frac{1}{2G}\left[\frac{A_{00}}{\alpha_{11}} - \frac{\alpha_{16}\alpha_{44} - \alpha_{46}\alpha_{14}}{\alpha_{11}(\alpha_{66}\alpha_{44} - \alpha_{64}\alpha_{46})} A_{02}\right]$$

$$C_{01} = \frac{1}{2G}\left[\frac{A_{01}}{\alpha_{33}} - \frac{\alpha_{03}(\alpha_{88}\alpha_{310} - \alpha_{810}\alpha_{)38}}{\alpha_{33}(\alpha_{1010}\alpha_{88} - \alpha_{108}\alpha_{810})}\right]$$

$$C_{02} = \frac{1}{2G}\frac{A_{02}\alpha_{44}}{\alpha_{66}\alpha_{44} - \alpha_{64}\alpha_{46}}$$

$$C_{20} = \frac{-1}{2G}\frac{A_{02}\alpha_{46}}{\alpha_{66}\alpha_{44} - \alpha_{64}\alpha_{46}} \qquad \text{(A-5)}$$

$$C_{21} = \frac{-1}{2G}\frac{A_{03}\alpha_{810}}{\alpha_{1010}\alpha_{88} - \alpha_{108}\alpha_{810}} \qquad \text{(A-5)}$$

$$C_{03} = \frac{1}{2G}\frac{A_{03}\alpha_{88}}{\alpha_{1010}\alpha_{88} - \alpha_{108}\alpha_{810}} \qquad \text{(A-5)}$$

The stress intensity factor is given by

$$K_I = \frac{8G}{ab}\left(\frac{\pi}{ab}\right)^{1/2}(a^2\sin^2\theta + b^2\cos^2\theta)^{1/4}$$

$$\left[C_{00} + \frac{C_{01}\sin\theta}{b} - \frac{4C_{20}\cos^2\theta}{a^2} - \frac{4C_{21}\cos^2\theta\sin\theta}{a^2 b} - \frac{4C_{02}\sin^2\theta}{b^2} - \frac{4C_{03}\sin^3\theta}{b^3}\right] \qquad \text{(A-6)}$$

where a and b are the major and minor axis of the elliptical crack, respectively, and θ is the elliptical angle which is positive in the counter clockwise direction and $\theta = 0$, zero on the major axis. α_{ij} are expressed in terms of the elliptical a and b. The quantities α_{ij} are defined as follows:

$$\alpha_{11} = \frac{4E(K)}{K'^2 A^3 t^3} \qquad K' = \frac{b}{a}, \quad A = \frac{a}{T}$$

$$\alpha_{14} = \frac{8}{A^5 T^5 K^2 K'^2}\left[K'^2 K(K) - (1-2K^2)E(K)\right]$$

$$\alpha_{16} = 8\,\frac{\left[(1+K^2)E(K) - K'^2 K(K)\right]}{A^5 T^5 K^2 K'^4}$$

$$\alpha_{44} = \frac{8}{A^7 T^7 K^2 K'^2}\left[\left(3 - 8K^2 + \frac{2}{K^2}\right)E(K) - 2K'^2\left(2 + \frac{1}{K^2}\right)K(K)\right]$$

$$\alpha_{46} = \frac{8}{A^7 T^7 K^4 K'^4}\left[K'^2(2-K^2)K(K) - 2(K'^2 + K^4)E(K)\right] \qquad \text{(A-7)}$$

$$\alpha_{66} = \frac{8}{A^7 T^7 K^4 K'^4}\left[2(3K^2-1)K(K) + \left(3K^2 + \frac{2-10K^2}{K'^2}\right)E(K)\right]$$

$$\alpha_{64} = \frac{8}{A^7 T^7 K^4 K'^4}\left[K'^2(2-K^2)K(K) - 2(K'^2 + K^4)E(K)\right]$$

$$\alpha_{33} = \frac{4}{A^5 T^5 K'^4 K^2}\left[(1+K^2)E(K) - K'^2 K(K)\right]$$

$$\alpha_{88} = \frac{8}{A^9 T^9 K'^4 K^6}\left[8K^4 K'^2 + 3K^2 K'^2 + 2K^2 - 8)E(K) + K'^2(4K^2 K'^2 + 5K'^2 + 3)K(K)\right]$$

$$\alpha_{310} = \frac{-8}{A^7 T^7 K'^4 K^4}\left[2(3K^2-1)K(K) + \left(3K^2 + \frac{2-10K^2}{K'^2}\right)E(K)\right]$$

$$\alpha_{38} = \frac{8}{A^7 T^7 K^4 K'^4}\left[2(K'^2 + K^4)E(K) - K'^2(2-K^2)K(K)\right]$$

$$\alpha_{810} = \frac{8}{A^9 T^9 K'^4 K^6}\left[(3K^2 K'^2 + 12K^2 - 8)K(K) + (6K^4 - 3K^2 + 16 - \frac{8}{K'^2})E(K)\right] + 16\frac{8}{K'^2}E(K)\Big]$$

$$\alpha_{1010} = \frac{8}{3A^9 T^9 K'^8 K^6}\left[(16K^2 - 45K^2 K'^2 + 8)K'^2 K(K) - (48 - 40K'^2 - 88K^2 K'^2 + 15K^2 K'^4)E(K)\right]$$

$$\alpha_{108} = \frac{8}{3A^9 T^9 K'^4 K^6}\left[(6K^4 - 3K^2 + 16 - \frac{8}{K'^2})E(K) + (3K'^2 K^2 + 12K^2 - 8)K(K)\right]$$

where

$K' = b/a$
$A = a/T$ (A-8)
$K^2 = 1 - K'^2$
$K(K)$ = the complete elliptical integral of the second kind.
$E(K)$ = the complete elliptical integral of the first kind.

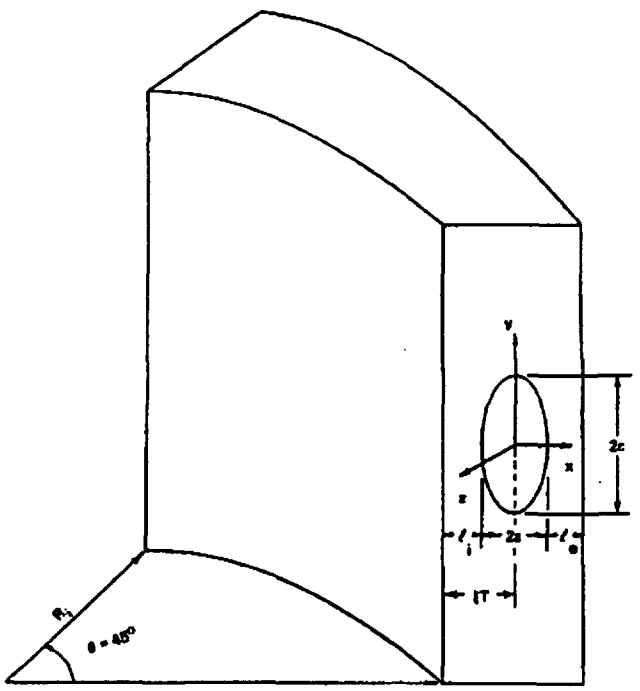

Figure 1. Cylindrical Pressure Vessel Containing a Buried Flaw

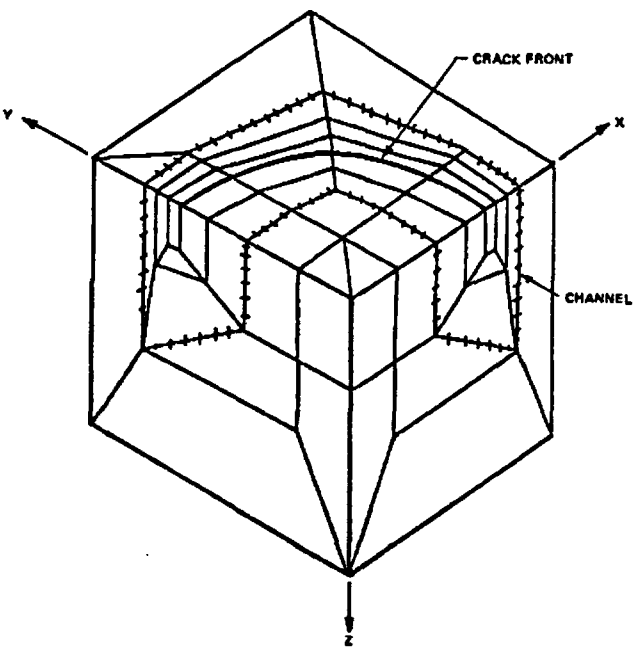

Figure 3. Undeformed Macroelement

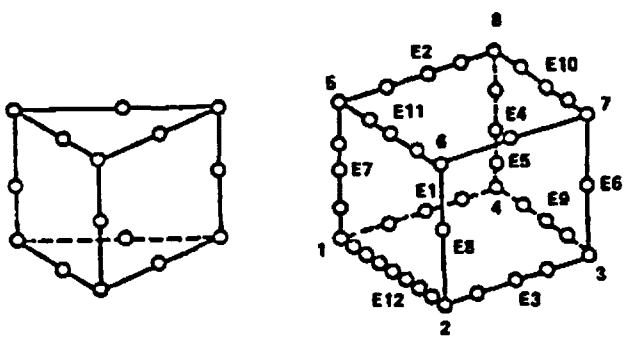

(a) 45 d.o.f. WEDGE (b) VARIABLE d.o.f. BLENDED BRICK

Figure 2. Micro Elements Used to Design the Macro Element

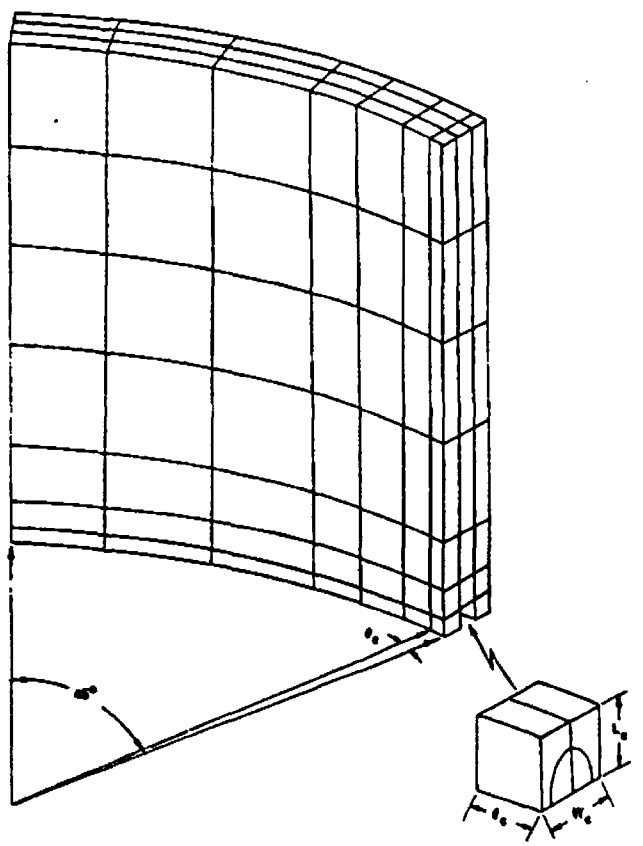

Figure 4. Finite Element Model of Cylinder with a Longitudinal Flaw, $\zeta = 1/2$

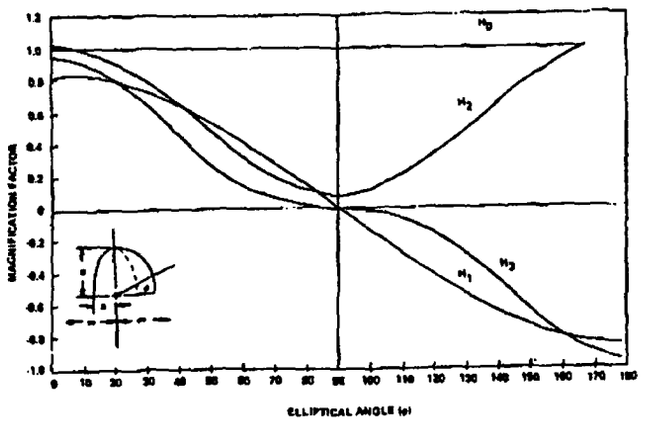

Figure 10. Magnification Factors for a Buried Flaw in an Infinite Medium

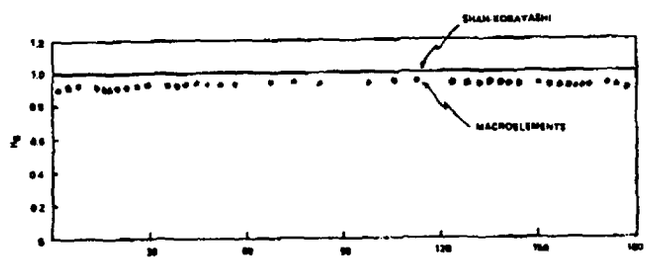

Figure 11. Comparison of H_0 Due to Macroelements and Shah-Kobayashi (19) Methods for a Buried Flaw in an Infinite Elastic Solid

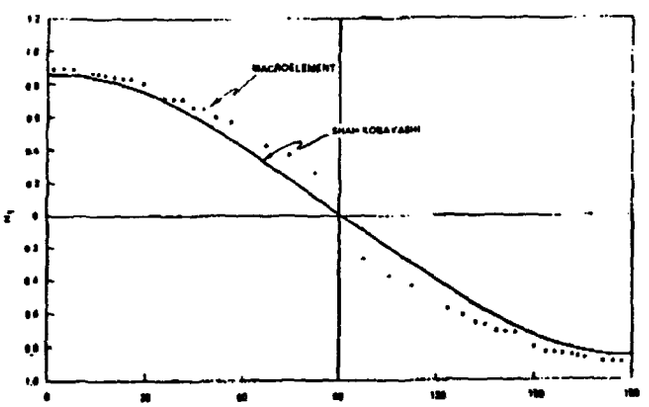

Figure 12. Comparison of H_1 Due to Macroelement and Shah-Kobayashi (19) Methods for a Buried Flaw in an Infinite Elastic Solid

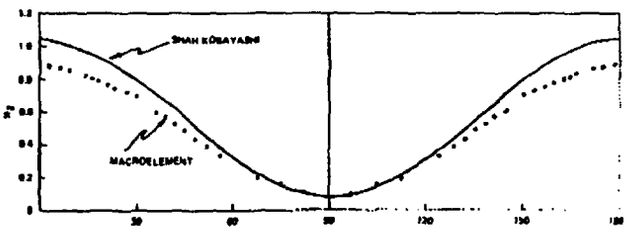

Figure 13. Comparison of H_2 Due to Macroelement and Shah-Kobayashi (19) Methods for a Buried Flaw in an Infinite Elastic Solid

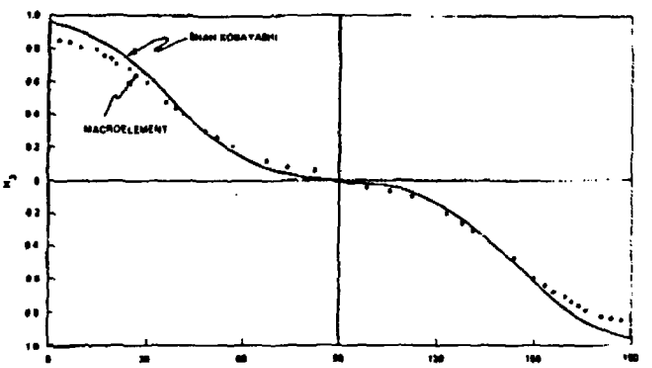

Figure 14. Comparison of H_3 Due to Macroelement and Shah-Kobayashi (19) Methods for a Buried Flaw in an Infinite Elastic Solid

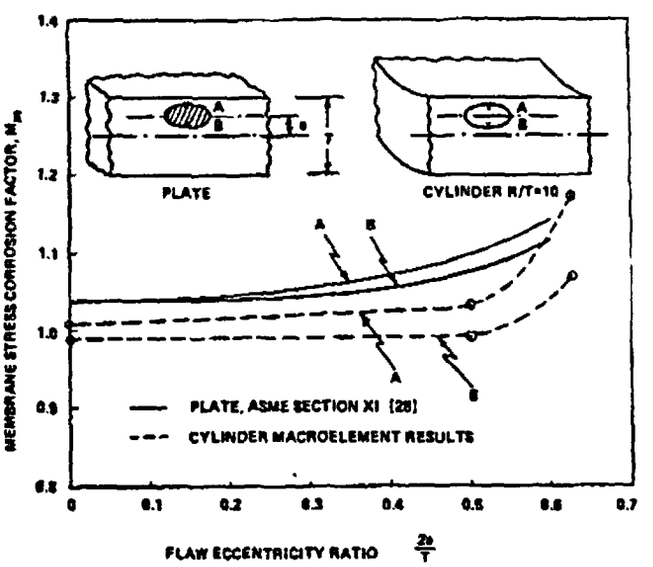

Figure 15. Comparison of Membrane Stress Correction Factors Due to ASME Code and Macroelement Method

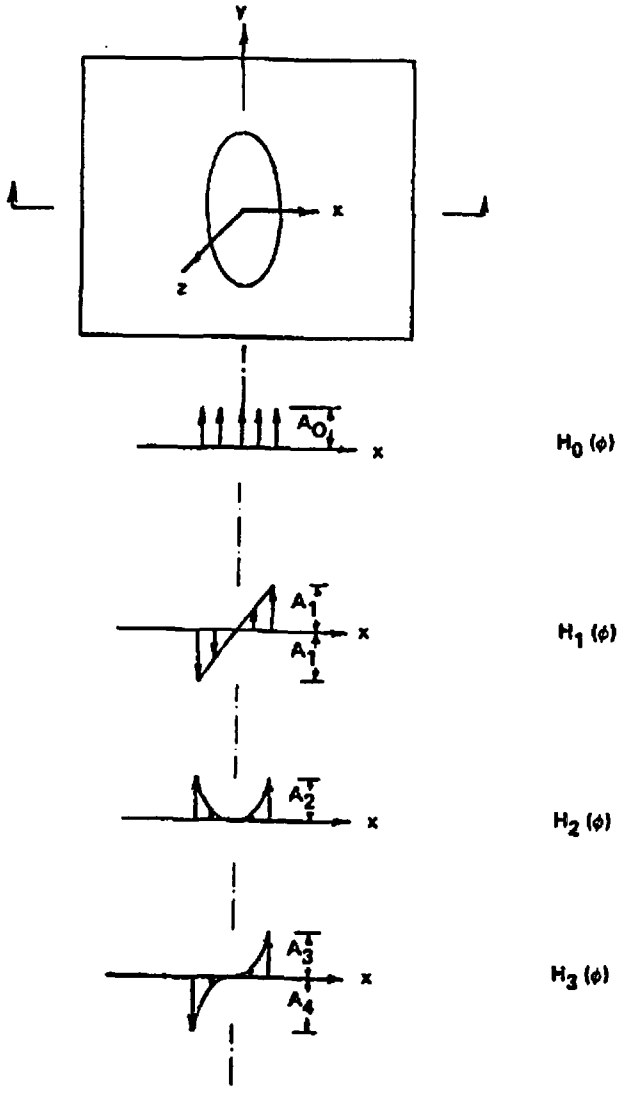

Figure 5. Distribution of Loading Components and the Associated Magnification Factors

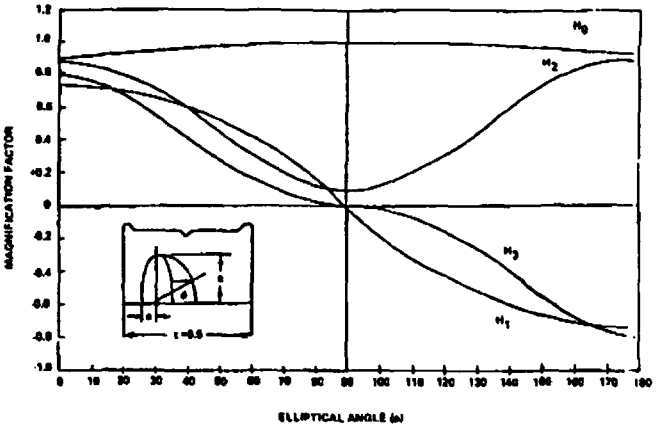

Figure 7. Magnification Factors for a Buried Elliptical Flaw Location at $\zeta = 1/4$

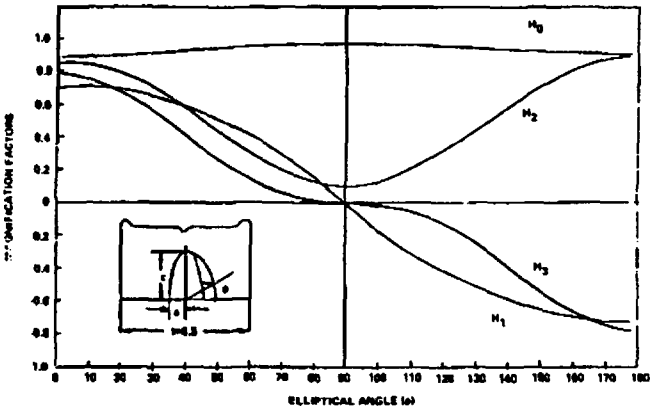

Figure 8. Magnification Factors for a Buried Flaw Located at $\zeta = 1/2$

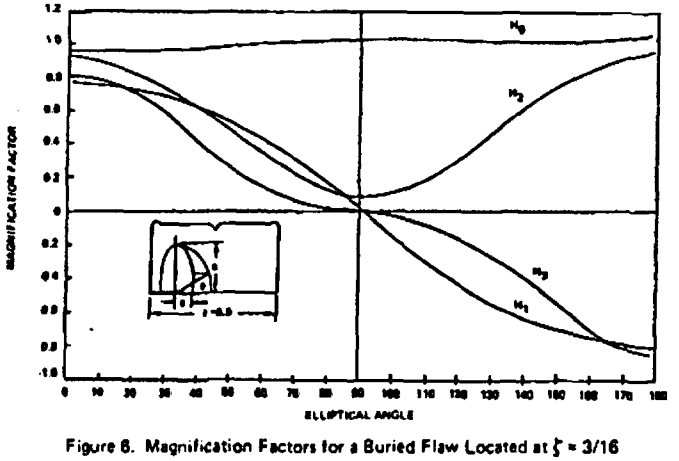

Figure 6. Magnification Factors for a Buried Flaw Located at $\zeta = 3/16$

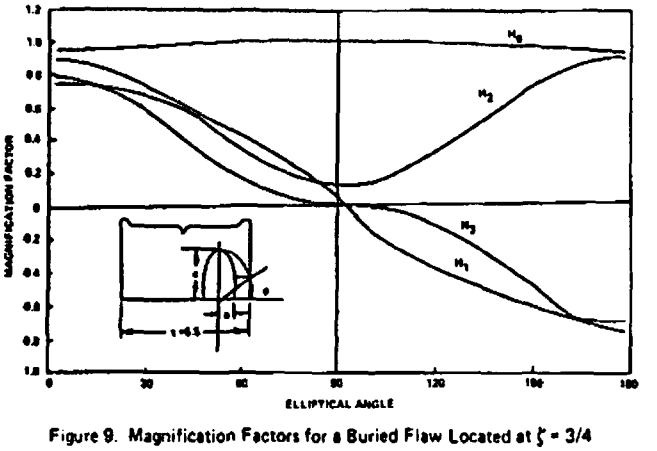

Figure 9. Magnification Factors for a Buried Flaw Located at $\zeta = 3/4$

ENCLOSURE 2

COVER LETTER TRANSMITTING NRC SER

UNITED STATES
NUCLEAR REGULATORY COMMISSION
WASHINGTON, D. C. 20555

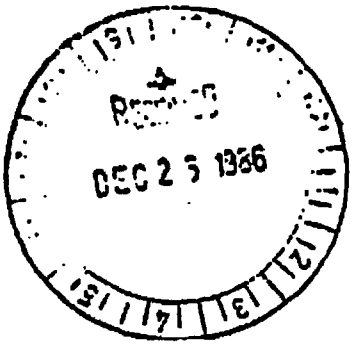

DEC 2 2 1986

Docket Nos. 50-282
and 50-306

Mr. D. M. Musolf, Manager
Nuclear Support Services
Northern States Power Company
414 Nicollet Mall
Midland Square, 4th Floor
Minneapolis, Minnesota 55401

Dear Mr. Musolf:

The Commission has completed the review of Northern States Power Company's (the licensee) request for an exemption to allow the application of the "leak-before-break" technology as a basis for the elimination of protective devices (i.e., pipe whip restraints, jet impingement barriers, and other related changes) of the primary reactor coolant systems at the Prairie Island Nuclear Generating Plant Unit Nos. 1 and 2. These protective devices were installed to mitigate the dynamic effects resulting from postulated large pipe ruptures. The technical information was provided by the licensee's letters dated October 24, 1984, October 21, and November 5, 1985 and supplemented by letter dated September 10, 1986 in response to staff concerns.

On April 11, 1986 a final rule was published in the Federal Register (51 FR 12502) amending 10 CFR Part 50, Appendix A, General Design Criteria (GDC) 4 that became effective on May 12, 1986. The revision of GDC 4 allows the use of analyses to eliminate from the design basis the dynamic effects of postulated pipe ruptures in the primary coolant system. The staff has completed the review of the licensee's submittals and concludes that the analysis of piping of primary coolant systems at the Prairie Island Nuclear Generating Plant Unit Nos. 1 and 2 is adequate and demonstrates compliance with the GDC 4 as amended. Therefore, an exemption to GDC 4 of Appendix A of 10 CFR Part 50 as amended that was requested by the licensee prior to the effective date of the rule is not necessary. On this basis, the removal of pipe whip restraints, jet impingement barriers, and other associated plant hardware may be implemented at your convenience. Our safety evaluation addressing this matter is enclosed.

This action completes our work effort under TAC Nos. 08731 and 08732.

Sincerely,

Dominic C. DiIanni, Project Manager
Project Directorate #1
Division of PWR Licensing-A

Enclosure:
Safety Evaluation

cc's: See Next Page